Nanoscale

Accepted Manuscript

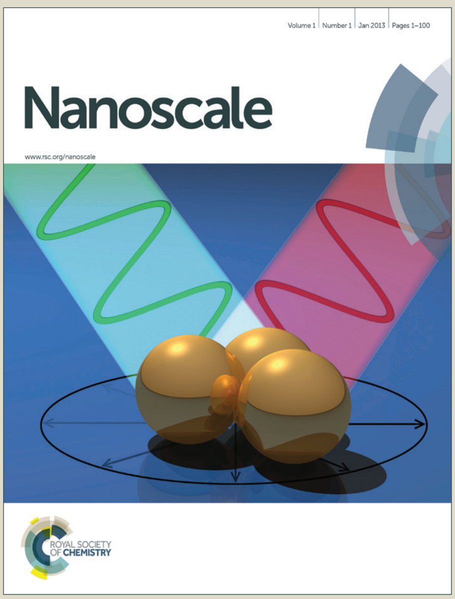

This is an *Accepted Manuscript*, which has been through the Royal Society of Chemistry peer review process and has been accepted for publication.

Accepted Manuscripts are published online shortly after acceptance, before technical editing, formatting and proof reading. Using this free service, authors can make their results available to the community, in citable form, before we publish the edited article. We will replace this *Accepted Manuscript* with the edited and formatted *Advance Article* as soon as it is available.

You can find more information about *Accepted Manuscripts* in the Information for Authors.

Please note that technical editing may introduce minor changes to the text and/or graphics, which may alter content. The journal's standard Terms & Conditions and the Ethical guidelines still apply. In no event shall the Royal Society of Chemistry be held responsible for any errors or omissions in this *Accepted Manuscript* or any consequences arising from the use of any information it contains.

ROYAL SOCIETY OF CHEMISTRY

www.rsc.org/nanoscale

Two-Dimensional TiS_2 Nanosheets for *in vivo* Photoacoustic Imaging and Photothermal Cancer Therapy

Xiaoxin Qian, Sida Shen, Teng Liu, Liang Cheng*, Zhuang Liu

Institute of Functional Nano & Soft Materials (FUNSOM), Collaborative Innovation Center of Suzhou Nano Science and Technology, Soochow University, Suzhou, Jiangsu 215123, China

E-mail: lcheng2@suda.edu.cn

Abstract:

Recently, transition metal dichalcogenides (TMDCs) have attracted significant attention in nanomedicine owing to their intriguing properties. In this study, TiS_2 nanosheets, a new TMDC nanomaterial, are synthesized by a bottom-up solution-phase method and then modified with polyethylene glycol (PEG), obtaining TiS_2-PEG with high stability in physiological solutions and no appreciable *in vitro* toxicity. Due to their high absorbance in the near-infrared (NIR) region, TiS_2-PEG nanosheets could offer strong contrast in photoacoustic imaging, which uncovers the high tumor uptake and retention of those nanosheets after systemic administration into tumor-bearing mice. We further apply TiS_2-PEG nanosheets for *in vivo* photothermal therapy, which is able to completely eradicate the tumors on mice upon intravenous injection of TiS_2-PEG and the followed NIR laser irradiation. Our work indicates that TiS_2 nanosheets with appropriate surface coating (e.g. PEGylation) would be promising new class of photothermal agent for imaging-guided cancer therapy.

Keywords: Transition metal dichalcogenides, TiS_2 nanosheets, photoacoustic imaging, photothermal therapy

Nanoscale Accepted Manuscript

Introduction

Photothermal therapy (PTT) as a new cancer treatment strategy has attracted much attention in recent years. By using near-infrared (NIR)-absorbing agents to convert light energy into heat and burn cancer, PTT shows significant advantages compared to traditional cancer treatment approaches such as surgery, chemotherapy, and radiotherapy in terms of minimal invasiveness and high efficacy [1, 2]. Recently, a large number of NIR-absorbing nanomaterials have been developed as photothermal agents for the treatment of cancer, such as gold nanomaterials[3-11], carbon-based nanomaterials[1, 12-15], copper sulfide nanoparticles[16-19], palladium nanosheets[20, 21], and some organic polymers and nano-assemblies of small organic molecules[22-24].

Two-dimensional (2D) nanomaterials with unusual physical and chemical properties have been extensively explored in materials science and engineering [25, 26]. Graphene, a 2D single layer of carbon atoms of honeycomb lattice structure, as a typical example, has shown exceptional electronic, optical, thermal, and mechanical properties[27, 28]. As the analogues of graphene, transition-metal dichalcogenides (TMDCs) such as MoS_2, $MoSe_2$, WS_2, WSe_2 and Bi_2Se_3, consisting of hexagonal layers of metal atoms sandwiched between two layers of chalcogen atoms, have also become a star in materials science in recent years, showing promising applications in many different areas including nanomedicine[25, 29-32]. Biosensing based on TMDCs has been demonstrated in a number of recent reports [33]. Several groups including ours have explored the use of TMDCs a new NIR absorbing agent for photothermal cancer treatment [31, 32, 34, 35], TMDCs nanosheets can also be used as a drug delivery platform due to the large specific surface area for cancer combination therapy[36-39].

Titanium dichalcogenides (TiS_2) is a typical class of TMDC materials and has also been studied recently in electronic devices or as a hydrogen-storage material [40-42]. Conventional TiS_2 thin films

Nanoscale Accepted Manuscript

are prepared using chemical vapor deposition (CVD)[41, 43]. Such a method involves decomposing different titanium and sulfur precursors on a substrate at temperatures exceeding 500 °C, and is relatively complicated and costly[40]. In this work, we synthesize TiS_2 nanosheets by a bottom-up solution-phase method with high product quality in a large scale, functionalize those nanosheets with polyethylene glycol (PEG), and for the first time utilize the obtained TiS_2–PEG as a new class of photothermal agent for in vivo photoacoustic imaging-guided tumor ablation, achieving great therapeutic efficacy on a mouse tumor model (**Figure 1**). Considering the biocompatibility of Ti and S elements, PEGylated TiS_2 NSs featured with strong NIR absorbance, efficient tumor passive homing ability, and low *in vitro* and *in vivo* toxicity, would be a promising new class of photothermal agent for cancer treatment.

Experiment section

Synthesis of TiS_2 nanosheets: A typical procedure is described as follows: 1 mmol $TiCl_4$ was added into a mixture of 20 ml oleylamine (OM) and 10 ml 1-octadecene (ODE) in a three-necked flask (50 ml) at room temperature. The solution was heated to 140 ^{o}C to remove water and oxygen under vigorous magnetic stirring in the presence of argon for protection for ~30 min. Afterwards, the temperature of the solution was rapidly raised to 300 ^{o}C and kept there for another 30 min in nitrogen atmosphere. An S/OM solution prepared by dissolving 2 mmol of S powders in 5 ml of OM was then injected into the flask at 300 ^{o}C within 10 min. The reaction was kept at 300 ^{o}C for 1 h. After being cooled down to room temperature, TiS_2 nanosheets were precipitated by adding excess ethanol (~30 ml), collected by centrifugation, and washed repetitively with ethanol.

Nanoscale Accepted Manuscript

Surface modification of TiS_2 NSs: PEG grafted poly(maleic anhydride-alt-1-octadecene) (C_{18}PMH-PEG) was synthesized following a literature procedure[44]. For PEGylation, 2 ml stock solution of TiS_2 (5 mg/ml) was precipitated by centrifuge. The nanosheets were washed twice with ethanol and dispersed in chloroform. Another solution of 20 mg C_{18}PMH-PEG polymer in 2 ml chloroform was then added. The mixture was stirred for 4 h. After blowing-dry chloroform, the residue was readily dissolved in water. The resultant solution was centrifuged to remove large aggregates to obtain TiS_2-PEG.

Characterization: The phase and crystallography of the products were characterized by using a PANalytical X-ray diffractometer equipped with Cuka radiation (λ=0.15406 nm). A scanning rate of 0.05 $^{o}s^{-1}$ was applied to record the pattern in the 2θ range of 10-80^{o}. Transmission electron microscopy (TEM) images of the NSs were obtained using a FEI Tecnai F20 transmission electron microscope equipped with an energy dispersive spectroscope (EDX) at an acceleration voltage of 200 kV. UV-vis-NIR spectra were obtained with PerkinElmer Lambda 750 UV-vis-NIR spectrophotometer. The size of the TiS_2-PEG nanosheets was measured by dynamic light scattering (DLS) (MALVERN ZEN3690).

Cell Culture experiments: 4T1 murine breast cancer cells were cultured in the standard cell medium recommended by American type culture collection (ATCC), under 37 ^{o}C within 5% CO_2 atmosphere. Cells seeded into 96 well plates were incubated with different concentrations of TiS_2-PEG for 24 h. Relative cell viabilities were determined by the standard methyl thiazolyl tetrazolium (MTT) assay. For in vitro photothermal therapy, 4T1 cancer cells were incubated with

Nanoscale Accepted Manuscript

and without TiS_2-PEG (25μg/mL) for 4h and then irradiated by an 808-nm laser at the power density of 0.8 W/cm^2 for 5 min. The cells were stained with Trypan blue for 30 min, washed with PBS, and then imaged under an optical microscope (Leica).

Tumor model: Balb/c mice were obtained from Nanjing Peng Sheng Biological Technology Co. Ltd and used under protocols approved by Soochow University Laboratory Animal Center. The 4T1 tumors were generated by subcutaneous injection of $1*10^6$ cells in ~30 μL serum-free RMPI-1640 medium onto the back of each female Balb/c mouse.

In vivo photoacoustic imaging: Photoacoustic imaging was performed with a preclinical photoacoustic computed tomography scanner (Endra Nexus 128, Ann Arbor, MI). During our experiments, anesthesia was maintained using pentobarbital (50 mg/kg). The mouse body temperature was maintained by using a water heating system at 37.5 ^{o}C. 4T1 tumor-bearing mice were intravenously (i. v.) injected with TiS_2-PEG nanosheets prior to imaging. During the imaging, the laser wavelength was about 800 nm.

In vivo photothermal therapy: Mice bearing 4T1 tumors 12 h post i. v. injection with TiS_2-PEG (2 mg/mL, 200 μL, dose = 20 mg/kg) were exposed to the 808-nm NIR laser (Hi-Tech Optoelectronics Co., Ltd. Beijing, China) at the power density of 0.8 W/cm^2 for 5 min. For control groups, mice were either treated with the same volume of saline before laser irradiation, or injected with TiS_2-PEG nanosheets but without laser exposure. The tumor surface temperatures were recorded by an IR thermal camera (IRS E50 Pro Thermal Imaging Camera). The tumor sizes were measured by a

Nanoscale Accepted Manuscript

caliper every the other day and calculated as the volume = (tumor length) × (tumor width)^2 /2. Relative tumor volumes were calculated as V/V_0 (V_0 was the tumor volume when the treatment was initiated).

Histology analysis: 30 days after i. v. injection of TiS_2-PEG (dose = 2 mg/kg), 3 mice from the treatment group and 3 age-matched female Balb/c control mice (without any injection of TiS_2-PEG NSs) were sacrificed by CO_2 asphyxiation for necropsy. Major organs from those mice were harvested, fixed in 10% neutral buffered formalin, processed into paraffin, sectioned at 8-micron thickness, stained with hematoxylin & eosin (H&E) and examined by a digital microscope (Leica QWin). Examined tissues include liver, spleen, kidney, heart, and lung.

Result and discussions

The synthesis of TiS_2, which was based on a previously reported protocol with slight modification[45], started by dissolving and heating up $TiCl_4$ precursor in a mixed solvent of oleylamine (OM) and 1-octadecene (ODE) under N_2 atmosphere. During this process, the titanium precursor solution gradually turned into dark red, probably because of the reaction between $TiCl_4$ and OM that gave rise to a Ti-OM complex. When the solvent temperature reached 300 ^oC, sulfur dissolved in OM was injected into the resulting solution. Upon injection of the sulfur solution, the solution color immediately turned into brown, suggesting the rapid formation of TiS_2.

The phase analysis of the as-prepared product was determined by power X-ray diffraction (XRD) (**Figure 2a**). All peaks in the spectrum were corresponding to the reflections of the cubic phase of TiS_2 and well matched with the reported results (JCPDs 88-2479). Transmission electron microscope

Nanoscale Accepted Manuscript

(TEM) image illustrated that the synthesized TiS_2 exhibited a sheet-like two-dimensional structure with a uniform size of ~100 nm (**Figure 2b**). The high-resolution TEM (**Figure 2c**) showed that the nanosheets have a lattice plane with a spacing of 0.254 nm, corresponding to the d spacing of the (011) plane of the hexagonal phase TiS_2. Besides the C, O, and Cu elements from the substrate, only peaks of Ti and S were detected in the EDS pattern (**Figure 2d**). Due to the hydrophobic OM coating on the surface of the TiS_2, amphiphilic polymers such as PEG-grafted Poly(maleic anhydride-alt-1-octadecene) (C_{18}PMH-PEG) could be used to modify TiS_2 through hydrophobic interactions to make those nanosheets water-soluble. The dynamic light scattering (DLS) data showed that the final size of TiS_2-PEG was ~100 nm **(Figure 2e)**. After surface modification, the obtained TiS_2-PEG exhibited excellent stability in various solutions, including saline, cell medium, and serum (**Figure 2f, inset**).

UV-vis-NIR spectrum of TiS_2 NSs (**Figure 2f**) showed broad absorption from UV to NIR. The extinction coefficient of the TiS_2-PEG at 808 nm was measured to be 26.8 $Lg^{-1}cm^{-1}$, which was similar to the previously reported TMDCs nanomaterials such as WS_2 and MoS_2[34, 36]. The high NIR absorbance of TiS_2-PEG NSs suggested that it would be an excellent photoabsorbing agent for potential photothermal therapy. In order to investigate the photothermal properties of TiS_2-PEG, solutions with various TiS_2 concentrations at 0.06, 0.12, 0.25, and 0.5 mg/mL were exposed to an 808-nm NIR laser at a power density of 0.8 W/cm^2. Obvious concentration-dependent temperature increase of TiS_2-PEG was found under laser irradiation (**Figure 2g&h**). The photothermal stability of TiS_2-PEG was also investigated, clearly demonstrating that those TiS_2-PEG nanosheets were very stable during the NIR irradiation (**Supporting Figure S1**).

Prior to the use of PEGylated TiS_2 nanosheets for *in vivo* imaging and therapy, we firstly tested

Nanoscale Accepted Manuscript

their cell cytotoxicity *via* the standard methyl thiazolyl tetrazolium (MTT) assay. No significant cytotoxicity of TiS_2-PEG to the murine breast cancer cells (4T1) was observed even under high concentrations up to 0.1 mg/mL (**Figure 3a**), suggesting that those nanosheets possess low cell cytotoxicity and good biocompatibility. Next, we used TiS_2-PEG as a photothermal agent for *in vitro* cancer cell ablation under laser irradiation. 4T1 cells were incubated with different concentrations of TiS_2-PEG for 6 h and then irradiated by the 808-nm laser with the power density of 0.8W/cm^2 (**Figure 3b**). The MTT results showed that as the increase of TiS_2-PEG concentrations, more cells were destroyed after laser irradiation (**Figure 3c**). Most cells were killed after being incubated with 0.1 mg/ml TiS_2-PEG under laser irradiation at 0.8 W/cm^2 for 5 min, indicating that TiS_2-PEG could serve as a rather effective photothermal agent.

Photoacoustic (PA) imaging is a non-invasive imaging modality offering increased in vivo imaging depth and spatial resolution compared to other traditional optical imaging methods[46-48]. We found that TiS_2-PEG with high NIR absorbance could be used as a great contrasting agent in photoacoustic imaging (**Figure 4a**). Balb/c female mice bearing 4T1 tumor were then *i.v.* injected with TiS_2-PEG. At the time points of 0, 2, 4, 8, 12, 24 h, photoacoustic imaging of the tumor was conducted (**Figure 4c**). While only major blood vessels could be seen in the tumor before the injection of TiS_2-PEG, strong photoacoustic signals showed up after i.v. injection of TiS_2-PEG and dispersed within the whole tumor **(Figure 4d)**, indicating the efficient accumulation of those nanosheets in the tumor likely owing to the enhanced permeability and retention (EPR) effect of cancerous tumors[24, 49, 50].

Next, we would like to use TiS_2-PEG as a photothermal agent for *in vivo* cancer treatment. Mice bearing 4T1 tumors were *i.v.* injected with TiS_2-PEG solution (2 mg/mL, 200 μl) or saline as control.

Nanoscale Accepted Manuscript

At 24 h post injection (p.i.), tumors on those mice were exposed to an 808-nm laser at the power density of 0.8 W/cm^2 for 5 min. The temperature changes of tumors were recorded by an infrared (IR) thermal camera **(Figure 5a)**. Owing to the strong NIR absorbance and efficient tumor accumulation of TiS_2-PEG, the tumor temperatures on mice injected with TiS_2-PEG quickly increased to ~65 ℃ within 5 min under NIR laser irradiation. In contrast, the surface temperature of tumors in mice injected with saline showed little change under the same irradiation condition.

The *in vivo* photothermal therapeutic effect of TiS_2-PEG was then evaluated. Balb/c mice bearing 4T1 tumors were separated into four groups with 5 mice per group after the tumor size reached about 60 mm^3.The mice in the treatment group were *i.v.* injected with TiS_2-PEG. After 24 h, the mice were exposed to the 808 nm laser at 0.8W/cm^2 for 5 min. The other three control groups included PBS injected mice with or without laser irradiation, and mice *i.v.* injected with TiS_2-PEG but without laser irradiation. It was found that tumors on mice with *i.v.* injection of TiS_2-PEG and laser irradiation disappeared 1 day after treatment, leaving black scars at the primary tumor sites which fell off in about 10 days **(Figure 5d)**. The tumor sizes of each group were measured every 2 days. Obviously, tumors of mice in the treatment group (TiS_2-PEG + laser irradiation) were completely ablated and no re-growth could be seen, while tumors in the other groups showed rapid growth (**Figure 5b**). The mice of three control groups died within 16 days while those after TiS_2-PEG induced photothermal therapy survived over 60 days (**Figure 5c**). Our results demonstrate that TiS_2-PEG is an efficient photothermal agent that can be used for *in vivo* cancer treatment.

At last, we explored the potential *in vivo* toxicity of TiS_2-PEG nanosheets. The behaviors of Balb/c mice were monitored after *i.v.* injection of TiS_2-PEG and PTT treatment. No single mouse death or any sign of toxic effect was observed within 60 days. Major organs were collected after

Nanoscale Accepted Manuscript

mice being sacrificed and then stained by hematoxylin and eosin (H&E) for histology analysis **(Figure 6)**. Our results have evidenced that TiS_2-PEG exerted no obvious toxicity to mice at our treatment dose, although further systematic studies are still needed to fully understand the detailed excretion and toxicology profiles of those nanosheets.

Conclusions

In summary, via a bottom-up method we have successfully synthesized TiS_2 nanosheets, which after surface functionalization with PEG are for the first time used for in vivo cancer imaging and therapy. It is found that PEGylated TiS_2 nanosheets exhibit excellent physiological stability and no obvious cell toxicity. Owing to the high NIR absorbance, our TiS_2-PEG not only can serve as a photothermal agent, but also could be used as a photoacoustic contrast agent. With high tumor uptake as revealed by *in vivo* photoacoustic imaging, TiS_2-PEG is then utilized for *in vivo* photothermal cancer treatment, achieving great therapeutic outcomes in our animal tumor model experiments. Preliminary results indicate no obvious toxicity of TiS_2-PEG to the treated mice. Compared with the other TMDCs explored for photothermal therapy such as MoS_2, WS_2 and Bi_2Se_3, Titanium in TiS_2 has been generally recognized such a biocompatible element (e.g. Titanium has been widely used in tissue engineering). Although further careful pharmacokinetics and long-term dose-dependent toxicology studies of TiS_2 are still required, PEGylated TiS_2 nanosheets presented in this work may be a promising nano-agent for cancer theranostics.

Acknowledgement

Nanoscale Accepted Manuscript

This work was partially supported by the National Natural Science Foundation of China (51302180, 51222203, 51002100, 51132006), the National "973" Program of China (2011CB911002, 2012CB932601), and a Project Funded by the Priority Academic Program Development of Jiangsu Higher Education Institutions. Liang Cheng was supported by a Post-doctoral research program of Jiangsu Province (1202044C) and a Post-doctoral science foundation of China (2013M531400). We thank Prof. Gang Liu in the Center for Molecular Imaging and Translational Medicine at Xiamen University for his great help in photoacoustic imaging.

Reference

1. J. T. Robinson, S. M. Tabakman, Y. Liang, H. Wang, H. Sanchez Casalongue, D. Vinh and H. Dai, *Journal of the American Chemical Society*, 2011, **133**, 6825-6831.
2. L. Cheng, C. Wang, L. Feng, K. Yang and Z. Liu, *Chemical Reviews*, 2014, **114**, 10869-10939.
3. R. Bardhan, S. Lal, A. Joshi and N. J. Halas, *Accounts of chemical research*, 2011, **44**, 936-946.
4. L. Dykman and N. Khlebtsov, *Chemical Society Reviews*, 2012, **41**, 2256-2282.
5. H. Liu, D. Chen, L. Li, T. Liu, L. Tan, X. Wu and F. Tang, *Angewandte Chemie*, 2011, **123**, 921-925.
6. Y. Xia, W. Li, C. M. Cobley, J. Chen, X. Xia, Q. Zhang, M. Yang, E. C. Cho and P. K. Brown, *Accounts of chemical research*, 2011, **44**, 914-924.
7. Z. Zhang, J. Wang and C. Chen, *Advanced Materials*, 2013, **25**, 3869-3880.
8. X. Yang, X. Liu, Z. Liu, F. Pu, J. Ren and X. Qu, *Advanced materials*, 2012, **24**, 2890-2895.
9. X. Huang, I. H. El-Sayed, W. Qian and M. A. El-Sayed, *Journal of the American Chemical Society*, 2006, **128**, 2115-2120.
10. H. Yuan, A. M. Fales and T. Vo-Dinh, *Journal of the American Chemical Society*, 2012, **134**, 11358-11361.
11. N. Wang, Z. Zhao, Y. Lv, H. Fan, H. Bai, H. Meng, Y. Long, T. Fu, X. Zhang and W. Tan, *Nano Res.*, 2014, **7**, 1291-1301.
12. K. Yang, L. Feng, X. Shi and Z. Liu, *Chemical Society Reviews*, 2013, **42**, 530-547.
13. M. Li, X. Yang, J. Ren, K. Qu and X. Qu, *Advanced Materials*, 2012, **24**, 1722-1728.
14. S. H. Hu, Y. W. Chen, W. T. Hung, I. W. Chen and S. Y. Chen, *Advanced Materials*, 2012, **24**, 1748-1754.
15. Y. Wang, K. Wang, J. Zhao, X. Liu, J. Bu, X. Yan and R. Huang, *Journal of the American Chemical Society*, 2013, **135**, 4799-4804.
16. Q. Tian, J. Hu, Y. Zhu, R. Zou, Z. Chen, S. Yang, R. Li, Q. Su, Y. Han and X. Liu, *Journal of the American Chemical Society*, 2013, **135**, 8571-8577.
17. Q. Tian, M. Tang, Y. Sun, R. Zou, Z. Chen, M. Zhu, S. Yang, J. Wang, J. Wang and J. Hu, *Advanced Materials*, 2011, **23**, 3542-3547.
18. X. Ding, C. H. Liow, M. Zhang, R. Huang, C. Li, H. Shen, M. Liu, Y. Zou, N. Gao and Z. Zhang, *Journal of the American Chemical Society*, 2014, **136**, 15684-15693.

Nanoscale Accepted Manuscript

19. B. Li, Q. Wang, R. Zou, X. Liu, K. Xu, W. Li and J. Hu, *Nanoscale*, 2014, **6**, 3274-3282.
20. X. Huang, S. Tang, X. Mu, Y. Dai, G. Chen, Z. Zhou, F. Ruan, Z. Yang and N. Zheng, *Nat Nano*, 2011, **6**, 28-32.
21. S. Tang, M. Chen and N. Zheng, *Nano Res.*, 2015, **8**, 165-174.
22. J. F. Lovell, C. S. Jin, E. Huynh, H. Jin, C. Kim, J. L. Rubinstein, W. C. Chan, W. Cao, L. V. Wang and G. Zheng, *Nature materials*, 2011, **10**, 324-332.
23. Z. Zha, X. Yue, Q. Ren and Z. Dai, *Advanced Materials*, 2013, **25**, 777-782.
24. L. Cheng, K. Yang, Q. Chen and Z. Liu, *ACS Nano*, 2012, **6**, 5605-5613.
25. J. N. Coleman, M. Lotya, A. O'Neill, S. D. Bergin, P. J. King, U. Khan, K. Young, A. Gaucher, S. De and R. J. Smith, *Science*, 2011, **331**, 568-571.
26. M. Chhowalla, H. S. Shin, G. Eda, L.-J. Li, K. P. Loh and H. Zhang, *Nature chemistry*, 2013, **5**, 263-275.
27. A. K. Geim, *science*, 2009, **324**, 1530-1534.
28. X. Li, W. Cai, J. An, S. Kim, J. Nah, D. Yang, R. Piner, A. Velamakanni, I. Jung and E. Tutuc, *Science*, 2009, **324**, 1312-1314.
29. D. Voiry, H. Yamaguchi, J. Li, R. Silva, D. C. Alves, T. Fujita, M. Chen, T. Asefa, V. B. Shenoy and G. Eda, *Nature materials*, 2013, **12**, 850-855.
30. Z. Zeng, T. Sun, J. Zhu, X. Huang, Z. Yin, G. Lu, Z. Fan, Q. Yan, H. H. Hng and H. Zhang, *Angewandte Chemie International Edition*, 2012, **51**, 9052-9056.
31. S. S. Chou, B. Kaehr, J. Kim, B. M. Foley, M. De, P. E. Hopkins, J. Huang, C. J. Brinker and V. P. Dravid, *Angewandte Chemie International Edition*, 2013, **52**, 4160-4164.
32. J. Li, F. Jiang, B. Yang, X.-R. Song, Y. Liu, H.-H. Yang, D.-R. Cao, W.-R. Shi and G.-N. Chen, *Sci. Rep.*, 2013, **3**.
33. C. Zhu, Z. Zeng, H. Li, F. Li, C. Fan and H. Zhang, *Journal of the American Chemical Society*, 2013, **135**, 5998-6001.
34. L. Cheng, J. Liu, X. Gu, H. Gong, X. Shi, T. Liu, C. Wang, X. Wang, G. Liu, H. Xing, W. Bu, B. Sun and Z. Liu, *Advanced Materials*, 2014, **26**, 1886-1893.
35. Y. Yong, L. Zhou, Z. Gu, L. Yan, G. Tian, X. Zheng, X. Liu, X. Zhang, J. Shi, W. Cong, W. Yin and Y. Zhao, *Nanoscale*, 2014, **6**, 10394-10403.
36. T. Liu, C. Wang, X. Gu, H. Gong, L. Cheng, X. Shi, L. Feng, B. Sun and Z. Liu, *Advanced Materials*, 2014, **26**, 3433-3440.
37. W. Yin, L. Yan, J. Yu, G. Tian, L. Zhou, X. Zheng, X. Zhang, Y. Yong, J. Li, Z. Gu and Y. Zhao, *ACS Nano*, 2014, **8**, 6922-6933.
38. T. Liu, C. Wang, W. Cui, H. Gong, C. Liang, X. Shi, Z. Li, B. Sun and Z. Liu, *Nanoscale*, 2014, **6**, 11219-11225.
39. J. Liu, X. Zheng, L. Yan, L. Zhou, G. Tian, W. Yin, L. Wang, Y. Liu, Z. Hu, Z. Gu, C. Chen and Y. Zhao, *ACS Nano*, 2015, **9**, 696-707.
40. C. Lin, X. Zhu, J. Feng, C. Wu, S. Hu, J. Peng, Y. Guo, L. Peng, J. Zhao and J. Huang, *Journal of the American Chemical Society*, 2013, **135**, 5144-5151.
41. J. Chen, S.-L. Li, Z.-L. Tao, Y.-T. Shen and C.-X. Cui, *Journal of the American Chemical Society*, 2003, **125**, 5284-5285.
42. V. V. Plashnitsa, F. Vietmeyer, N. Petchsang, P. Tongying, T. H. Kosel and M. Kuno, *The Journal of Physical Chemistry Letters*, 2012, **3**, 1554-1558.
43. C. J. Carmalt, S. A. O'Neill, I. P. Parkin and E. S. Peters, *Journal of Materials Chemistry*, 2004, **14**, 830-834.
44. L. Cheng, W. He, H. Gong, C. Wang, Q. Chen, Z. Cheng and Z. Liu, *Advanced Functional Materials*, 2013, **23**, 5893-5902.
45. L. Cheng, W. Huang, Q. Gong, C. Liu, Z. Liu, Y. Li and H. Dai, *Angewandte Chemie International Edition*,

Nanoscale Accepted Manuscript

2014, **53**, 7860-7863.
46. C. Kim, C. Favazza and L. V. Wang, *Chemical reviews*, 2010, **110**, 2756-2782.
47. K. H. Song, C. Kim, C. M. Cobley, Y. Xia and L. V. Wang, *Nano letters*, 2008, **9**, 183-188.
48. S. K. Maji, S. Sreejith, J. Joseph, M. Lin, T. He, Y. Tong, H. Sun, S. W.-K. Yu and Y. Zhao, *Advanced Materials*, 2014, **26**, 5633-5638.
49. L. Cheng, K. Yang, Y. Li, J. Chen, C. Wang, M. Shao, S.-T. Lee and Z. Liu, *Angewandte Chemie International Edition*, 2011, **50**, 7385-7390.
50. K. Yang, S. Zhang, G. Zhang, X. Sun, S.-T. Lee and Z. Liu, *Nano Letters*, 2010, **10**, 3318-3323.

Nanoscale Accepted Manuscript

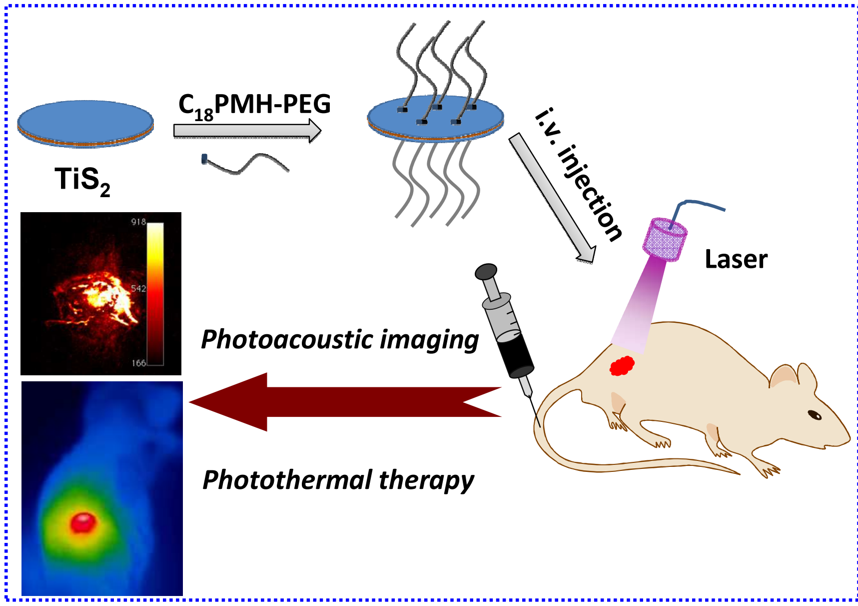

Figure 1. Scheme of using TiS_2-PEG nanosheets for photoacoustic imaging guided photothermal therapy.

Nanoscale Accepted Manuscript

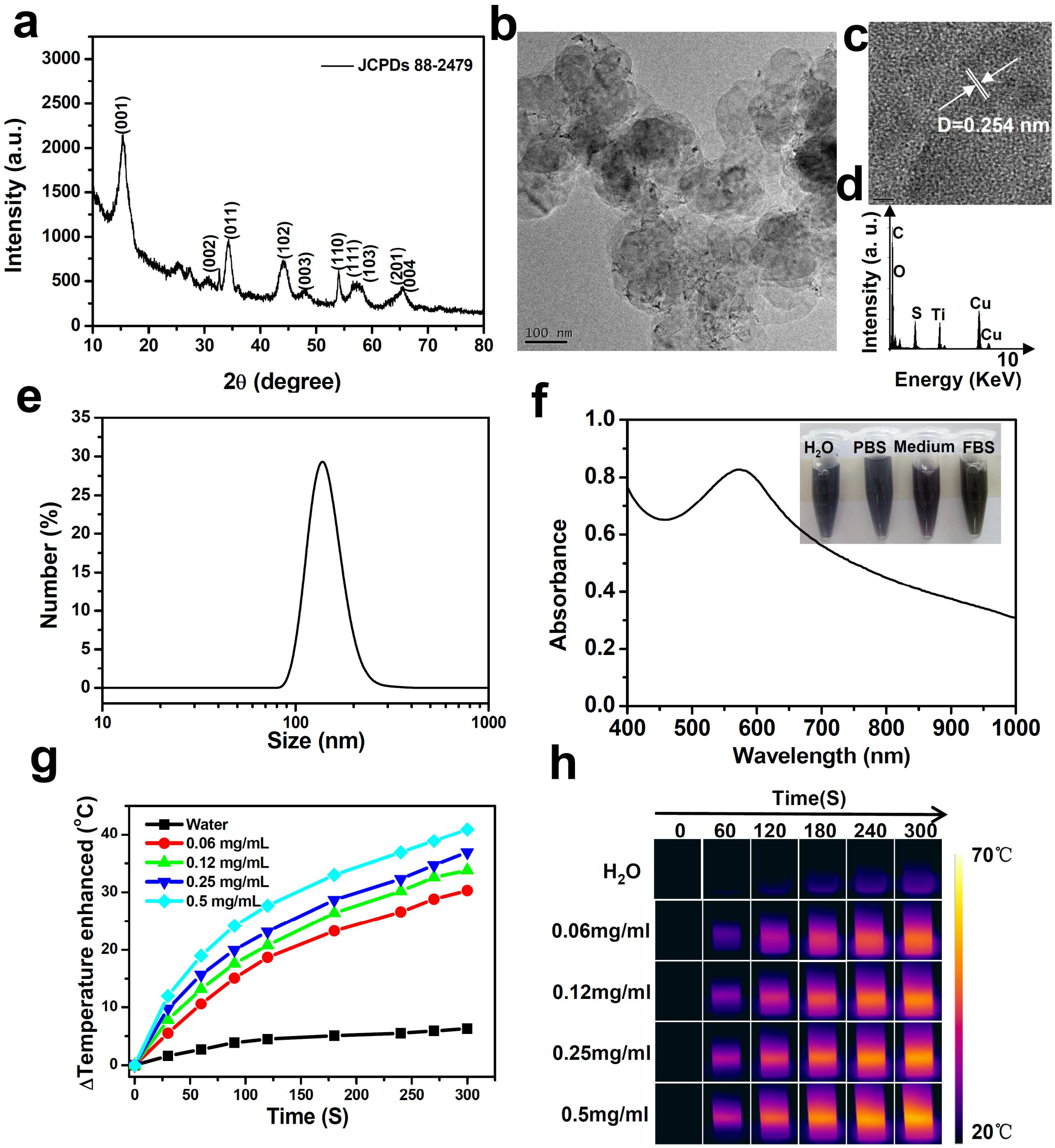

Figure 2. Characterization of PEGylated TiS_2 nanosheets. **(a)** XRD spectrum of as-made TiS_2 nanosheets. **(b-d)** TEM image **(b)**, HR-TEM image **(c)**, and EDS spectrum **(d)** of as-made TiS_2 nanosheets. **(e)** DLS size distribution of PEGylated TiS_2 nanosheets. **(f)** UV-vis-NIR absorbance spectra of TiS_2–PEG in water. Inset: Photos of TiS_2-PEG in various physiological solutions. **(g&h)** Photothermal heating curves **(g)** and IR thermal images **(h)** of pure water and TiS_2-PEG solutions with different concentrations (0.06, 0.12, 0.25, and 0.5 mg/mL) under 808-nm laser irradiation at the power density of 0.8 W/cm^2.

Nanoscale Accepted Manuscript

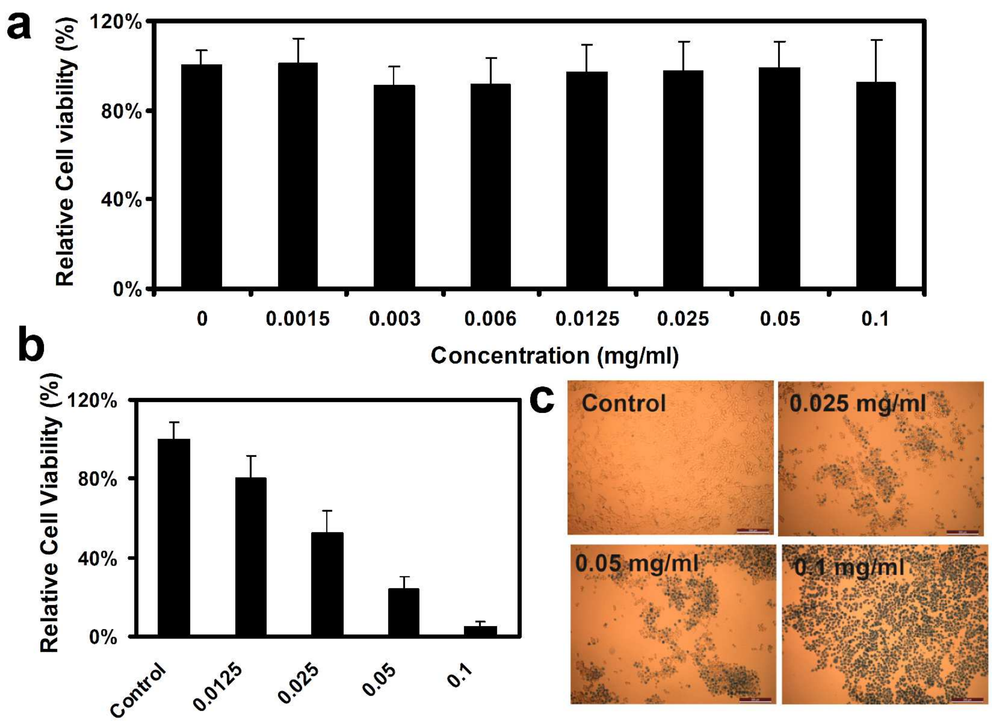

Figure 3. In vitro cell culture experiments. **(a)** Relative viabilities of 4T1 cells after being incubated with various concentrations of TiS_2-PEG for 24 h. **(b)** Relative viabilities of 4T1 cells after incubation with different concentrations of TiS_2-PEG and then being exposed to the 808-nm laser at the power density of 0.8 W/cm^2 for 5 min. **(c)** Optical microscopy images of Trypan blue stained cells after incubated with different concentrations of TiS_2-PEG and the followed laser irradiation.

Nanoscale Accepted Manuscript

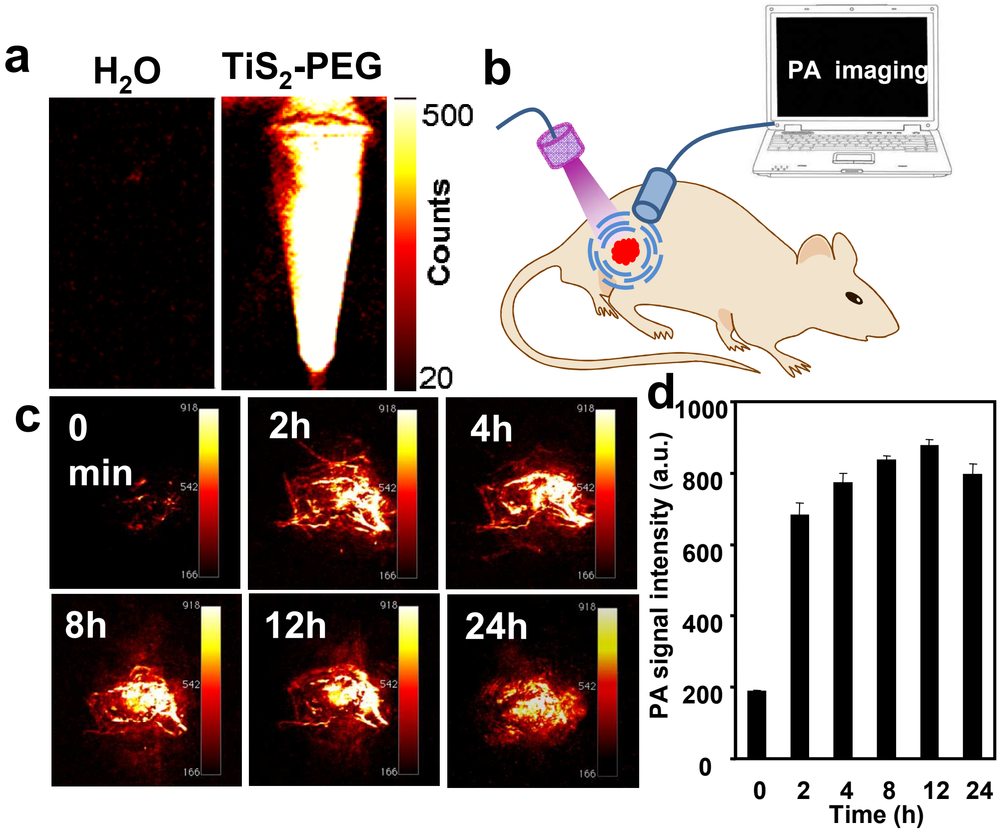

Figure 4 In vivo photoacoustic imaging in 4T1-tumor bearing mice. **(a)** Photoacoustic images of water (left) and a TiS_2-PEG solution (right). **(b)** Scheme of the mice after intravenous injection of TiS_2-PEG for photoacoustic imaging. **(c&d)** Photoacoustic images**(c)** and photoacoustic signal **(d)** of tumors on mice taken at different time points after i.v. injection of TiS_2-PEG

Nanoscale Accepted Manuscript

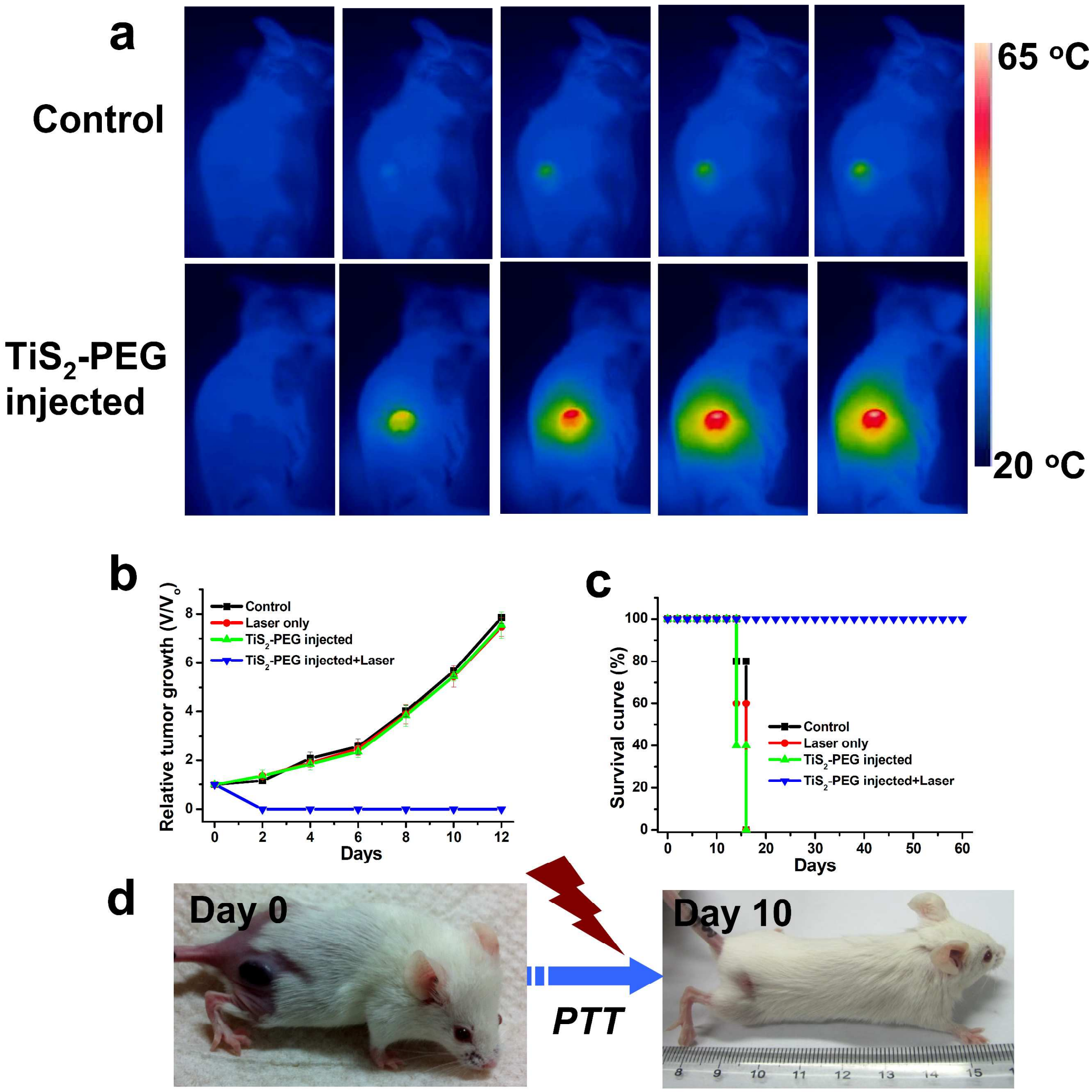

Figure 5 In vivo photothermal therapy. **(a)** Infrared thermal images of 4T1 tumor-bearing mice with i.v injection of TiS_2-PEG solution (2 mg/mL, 200 µl) under laser irradiation at the power density of 0.8 W/cm^2 for 5 min (24 h post injection). **(b)** The growth of 4T1 tumors in different groups of mice after various treatments indicated. The relative tumor volumes were normalized to their initial sizes. For the treatment groups, mice i.v. injected with TiS_2 -PEG at 24 h p.i. (n = 5), were exposed to the 808-nm laser (0.8 W/cm^2, 5 min).Three other groups of mice were used as controls: saline (n = 5); laser only without TiS_2 -PEG injection (n = 5); i.v. injected TiS_2-PEG without laser irradiation (n =5). Error bars were based on standard error of mean (SEM). **(c)** Survival curves of mice after various treatments as indicated in **(b)**. **(d)** Photographs of tumor-bearing mice with i.v injection of TiS_2-PEG (12 h p.i.) before laser irradiation (left) and 10 days after photothermal treatment (right).

Nanoscale Accepted Manuscript

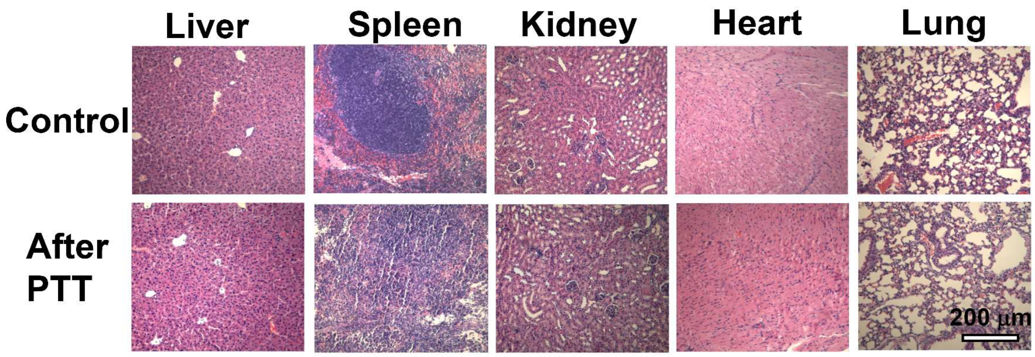

Figure 6. H&E stained images of major organs from untreated healthy mice and TiS_2-PEG treated 40 days after photothermal therapy (with tumors eliminated). No noticeable damage was observed in major organs including liver, spleen, kidney, heart, and lung.

Nanoscale Accepted Manuscript

Nanoscale Accepted Manuscript